Bridging the pressure and materials gaps between catalysis and surface science: clean and modified oxide surfaces

H.-J. Freund, H. Kuhlenbeck, J. Libuda, G. Rupprechter, M. Bäumer and H. Hamann

Fritz-Haber-Institut der Max-Planck-Gesellschaft, Faradayweg 4-6, D-14195 Berlin, Germany

The preparation of model systems based on thin epitaxial oxide films and oxide single crystals is discussed. A variety of surface sensitive techniques has been applied to study the geometric and electronic properties of these systems. The findings are correlated with adsorption and reaction of probe molecules on the surfaces. Metal vapor deposition under controlled conditions leads to the formation of metal aggregates with narrow size distributions. Their properties have been characterized, establishing that we can begin to bridge the materials gap between catalysis and surface science. While mainly performed under UHV conditions, adsorption measurements can be pushed to ambient conditions using non-linear optical techniques such as sum frequency generation. Results for systems with deposited metal aggregates will be discussed.

KEY WORDS: model catalysts; oxide surfaces; metal clusters on oxide surfaces; pressure gap; materials gap

1. Introduction

Catalysts are rather complex materials. Their surface structure is very difficult to study, in particular under working conditions, i.e., ambient or elevated gas pressure. Understanding catalysis at the atomic level is a formidable task. Whether it is possible at all has still to be shown. Surface science has to a large extent been driven by catalysis. With the development of a whole arsenal of surface analytical tools, the past 35 years of surface science have seen significant progress, although the final goal of understanding catalysis at the atomic level has, of course, not been attained [1]. Several gaps between catalysis and traditional surface science have been identified:

(1) the materials gap,

(2) the pressure gap,

(3) the complexity gap.

Surface science has reached a degree of maturity that allows us to bridge these gaps in part [2,3]. Using model systems with increasing degree of complexity [4] or even model catalysts is one strategy to try to bridge the materials gaps. Closing the pressure gap can be achieved by virtue of surface sensitive techniques that work in the presence of a gas phase, such as TDS, IRAS, ESR, SFG, STM, X-ray scattering and X-ray absorption [5]. Closing the complexity gap has to involve further methods to study gas and mass transport.

In order to start bridging the materials gap, several groups have turned towards the study of oxide surfaces. In the following we will address several examples, looking at the reactivity of molecules, in particular oxygen, on oxide surfaces as well as at structure–reactivity relations in the systems. We then move one step further to modify oxide surfaces with deposited metal aggregates and study adsorption and reaction on such systems under UHV conditions. Then techniques are applied for the study of such complex systems that allow us to look at adsorption under higher gas pressures in an attempt to bridge the pressure gap [6–8].

2. Oxide surfaces

The preparation of a clean oxide surface in ultrahigh vacuum is a rather difficult task. Strictly speaking, a certain oxygen activity is necessary in the gas phase to establish true equilibrium and then the stoichiometry is defined according to the chosen conditions [9]. In this respect, the oxide stoichiometry is not well-defined under dynamical UHV conditions, and the system is only kinetically stabilized. It is therefore believed that defects determine the physical and chemical properties of oxide surfaces. Particularly interesting are vanadium oxides and vanadylpyrophosphate compounds [10,11]. Activation of hydrocarbons is thought to take place through abstraction of hydrogen atoms and the formation of surface hydroxyl groups involving defects and isolated transition metal oxide cluster sites [12]. Conceptual studies in this area have been pioneered by Grasselli and his collaborators [10–12].

We have started to study various vanadium oxide surfaces, V_2O_5, VO_2 [13] and V_2O_3 [14]. Figure 1 shows a photoemission spectrum of $V_2O_5(001)$ at the top which may be interpreted on the basis of calculations by Hermann and his group [15]. Briefly, the spectrum is dominated by O 2p/O 2s emissions and there is a minor admixture of the V 3d wave functions in the panel showing the results of the calculations. There are no features near the Fermi energy which would, if they were present, be characteristic for defects leaving V atoms in lower oxidation states. The oxygen derived part of the valence band can be separated into contributions from the various types of oxygens constituting the structure, as shown in the right part of figure 1. The terminal vanadyl oxygen [O(1)] gives rise to the central features

1022-5528/01/0600-0201$19.50/0

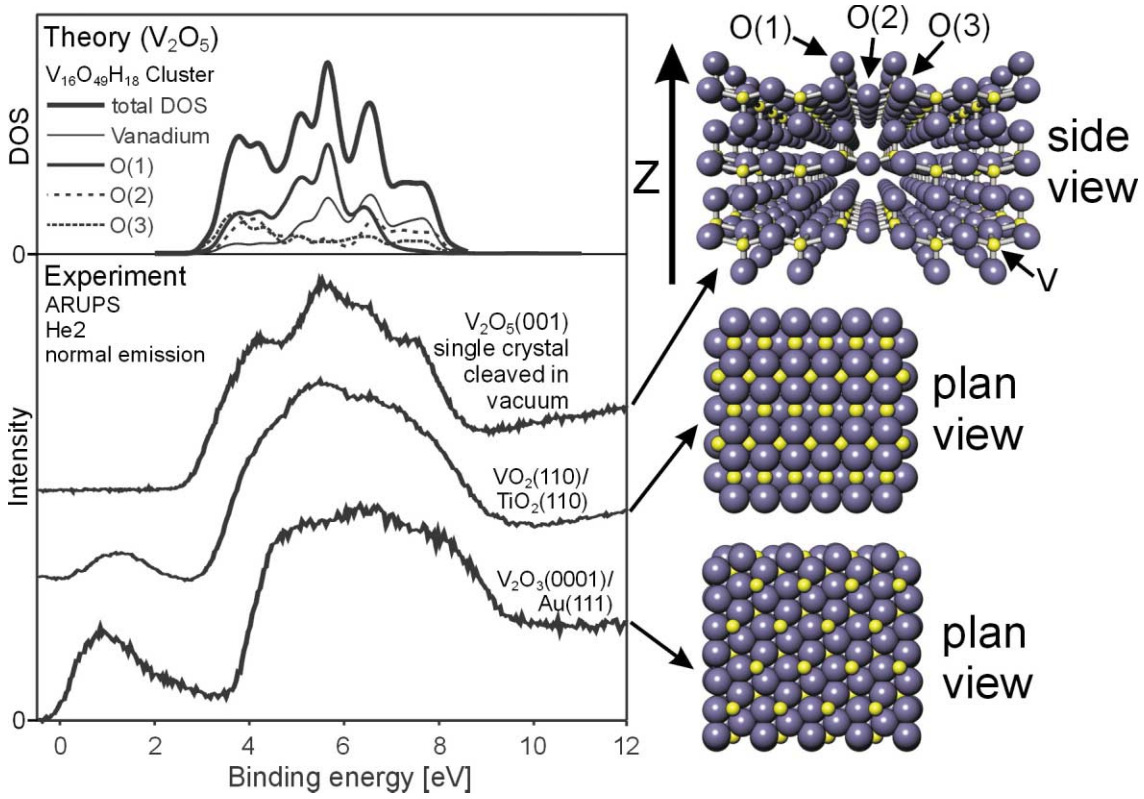

Figure 1. Photoelectron spectra and schematic representations of structures of various vanadium oxides [13,14]. For comparison a computed density of states [15] is shown.

whereas the bridging oxygens [O(2) and O(3)] connecting the vanadyl groups are contributing to the wings of the valence band. We will use this fact to identify oxygen specific reactivity. The spectrum in the panel below V_2O_5 is that of VO_2. VO_2(110) has been grown as a thin film on the isostructural rutile(110) surface. The oxygen derived valence band is slightly different from that of V_2O_5. A characteristic difference is the appearance of a feature close to the Fermi edge in VO_2 indicating the presence of vanadium 3d electrons. Its intensity represents to some extent the population of the V 3d orbitals. When we turn from VO_2 to V_2O_3 an even stronger increase in the V 3d intensity is observed. In figure 1, in the lower panel, the valence band photoemission spectrum of V_2O_3(0001)/Au(111) is shown. The V_2O_3 film shows a sharp hexagonal LEED pattern representing the corundum type structure similar to Al_2O_3, Cr_2O_3 and Fe_2O_3 (see below). Again, the V_2O_3 oxygen valence band emission is not very characteristic, as compared with VO_2 and V_2O_5. It is only the change in the near Fermi edge structures that show a characteristic variation from V^{5+} to V^{3+}.

Vanadium pentoxide is rather inactive with respect to adsorbates. For example, molecular hydrogen only leads to observable effects in the photoelectron spectrum after 10^4 L exposure. On the other hand, atomic hydrogen leads already at low exposure to recognizable changes in the photoelectron spectrum. The spectrum shown in figure 2 in the middle has been obtained after exposing the surface to atomic hydrogen. Opposite to the finding with molecular hydrogen the surface is chemically corroded. Defects form, as we also

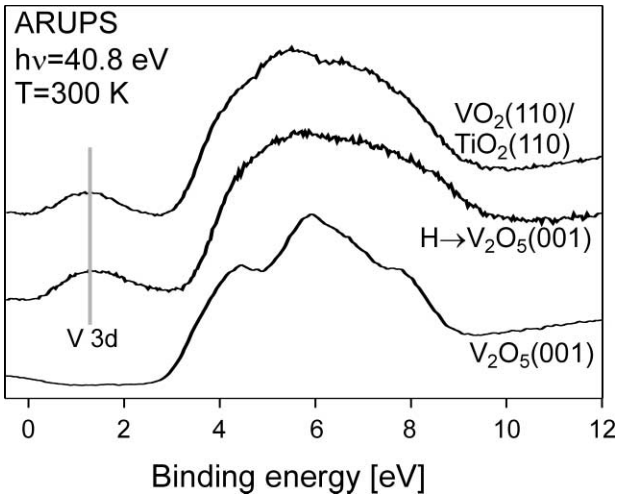

Figure 2. Photoelectron spectra of V_2O_5(001) and VO_2(110)/TiO_2(110) in comparison with a photoelectron spectrum obtained after dosing atomic hydrogen to a V_2O_5(001) surface.

know from electron energy loss spectroscopy, and concomitantly reduced metal centers show up near the Fermi edge. In fact, the spectrum looks very similar to the one of VO_2 which we show for comparison. We have investigated the surface with vibrational spectroscopy and found no indication for the formation of hydroxyls. It is very likely, that during exposure water evolves from the surface. Still the complete absence of OH on the surface is surprising and might point to the formation of hydrogen vanadium oxide

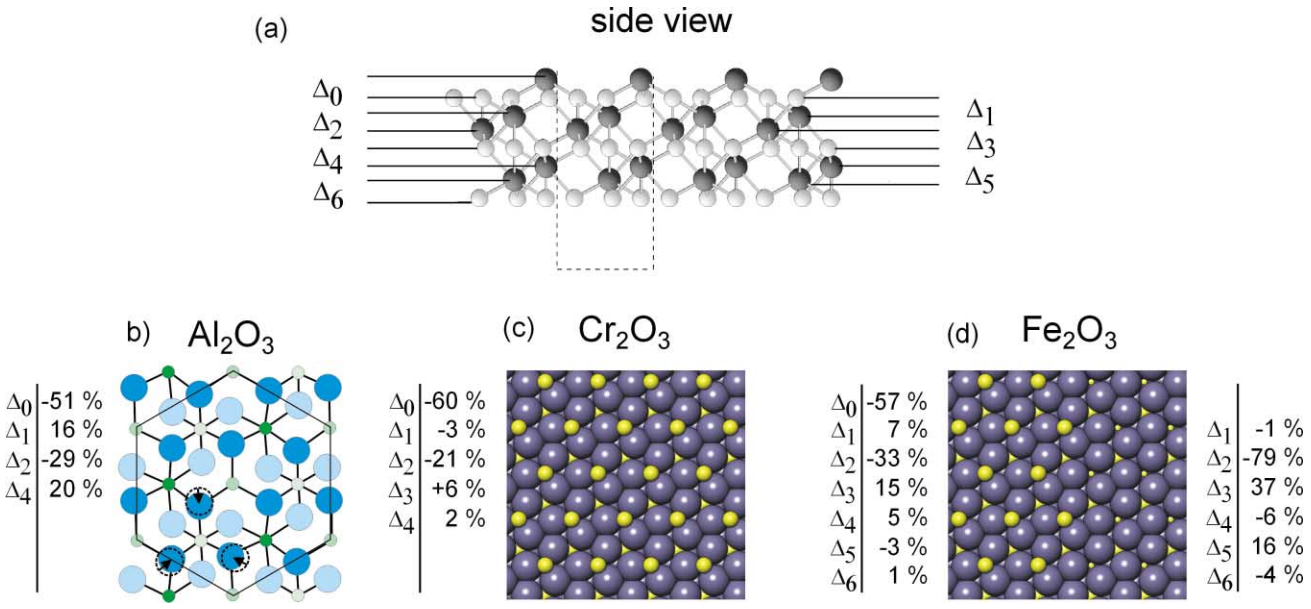

Figure 3. Experimental data on the structure of corundum-type depolarized (0001) surfaces (side and top views). Adapted from (b) [17], (c) [18] and (d) [19].

bronzes which are well-known to exist and which also have been used as precursors in the preparation of catalysts [16]. We are now starting to investigate reactivity of these surfaces to more complex molecules.

The best studied oxide surfaces are those of TiO_2, the rocksalt structured MgO and NiO as well as the corundum structured Al_2O_3, Cr_2O_3 and Fe_2O_3. Figure 3 shows the results of structural determinations for the three related systems $Al_2O_3(0001)$ [17], $Cr_2O_3(0001)$ [18] and $Fe_2O_3(0001)$ [19]. In all cases a stable structure in UHV is the metal ion terminated surface retaining only half of the number of metal ions in the surface as compared to a full buckled layer of metal ions within the bulk [20]. The interlayer distances are very strongly relaxed down to several layers below the surface [21]. The perturbation of the structure of oxides due to the presence of the surface is considerably more pronounced than in metals, where the interlayer relaxations are typically of the order of a few percent. The absence of the screening charge in a dielectric material such as an oxide contributes to this effect considerably. It has recently been pointed out that oxide structures may not be as rigid as one might think judged on the relatively stiff phonon spectrum in the bulk [22,23]. In fact, at the surface the phonon spectrum may become soft so that the geometric structure becomes rather flexible, and thus also very much dependent on the presence of adsorbed species [23].

The vibration modes of a clean $Cr_2O_3(0001)$ surface have been studied under ultrahigh vacuum conditions with high resolution electron energy loss spectroscopy [23]. Figure 4 shows the spectrum of the clean surface at the bottom. A mode, which is confined to the first few atomic layers of the oxide, was detected, in addition to the Fuchs–Kliewer phonons, at 21.4 meV. This mode shows only a very small isotopic shift when the $Cr_2O_3(0001)$ film is prepared from $^{18}O_2$ instead of $^{16}O_2$. In contrast to the Fuchs–Kliewer

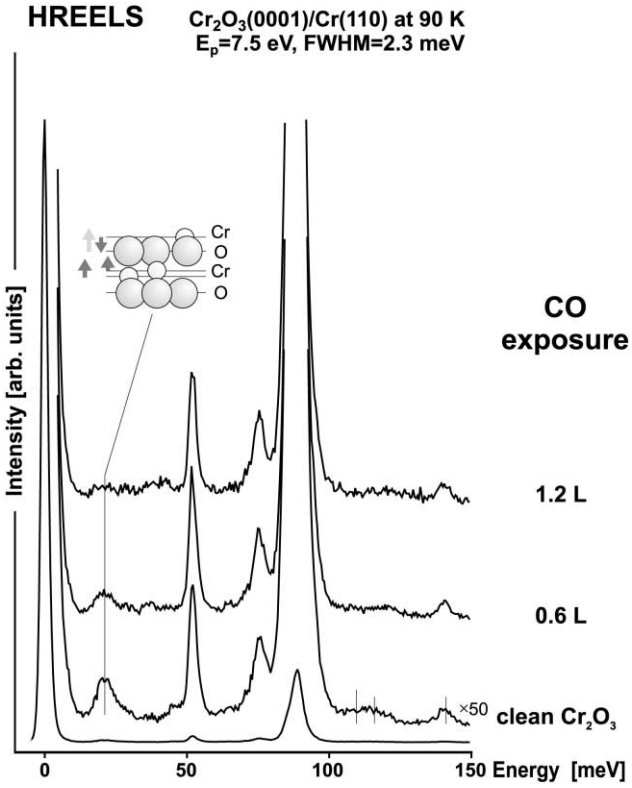

Figure 4. Electron energy loss spectra in the vibrational regime of clean and CO-covered $Cr_2O_3(0001)/Cr(110)$ surface (E_p 7.5 eV, specular scattering). The inset shows a schematic representation of the calculated normal mode of a $Cr_2O_3(0001)$ surface at 21.4 meV, according to [23].

phonons which extend deeply into the bulk the 21.4 meV mode is very sensitive towards the presence of adsorbates, as is shown in figure 4. This can be seen by its attenuation upon exposure of the surface to CO, which in this case is

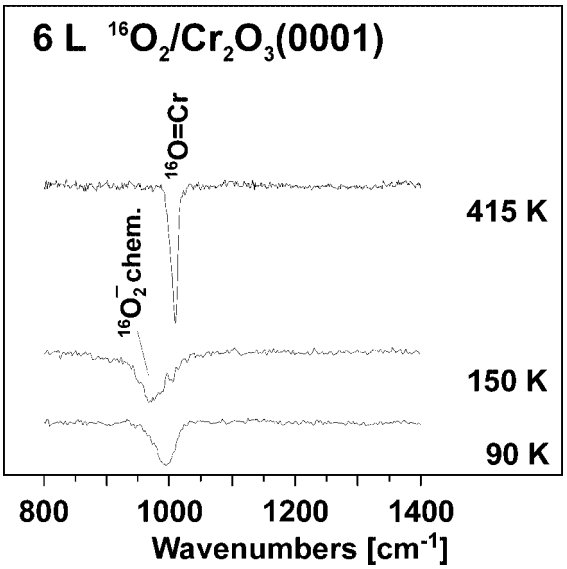

Figure 5. IRAS spectra after adsorption of a saturation coverage of O_2 on Cr_2O_3(0001)/Cr(110). The spectrum at the bottom was taken at 90 K. Other spectra are taken at the temperatures indicated.

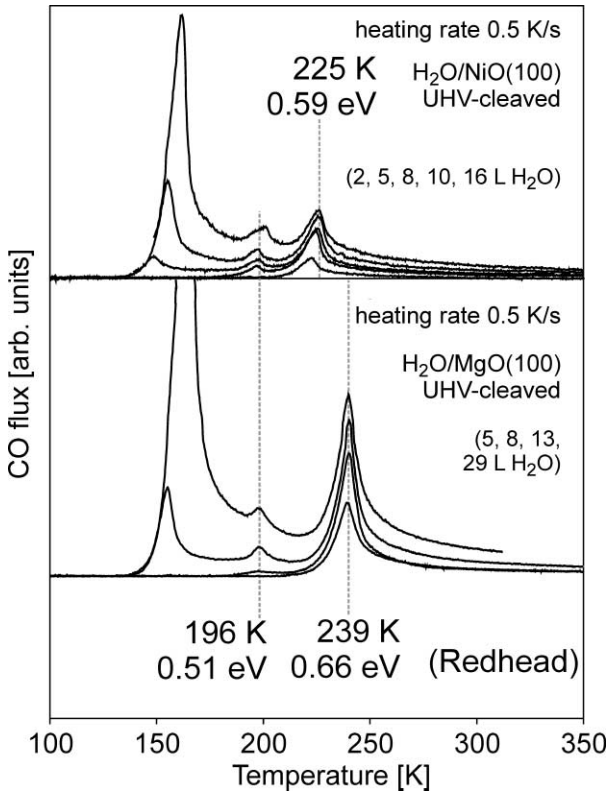

Figure 6. Thermal desorption spectra of H_2O on UHV-cleaved MgO(100) and NiO(100) surfaces. Maxima are indicated and the energies given have been calculated according to the Redhead formula.

only weakly adsorbed. Full-potential linearized augmented plane wave calculations [23] show that this mode is an in-phase oscillation of the second-layer oxygen atoms and the Cr atoms of the two layers below. A schematic representation of the mode is shown in the inset of figure 4.

Bulk oxide stoichiometries depend strongly on oxygen pressure, a fact that has been recognized for a long time and we have alluded to above [21]. So do oxide surfaces, structures and stoichiometries, a fact that has been shown again in a recent study on the Fe_2O_3(0001) surface by the Scheffler and Schlögl groups [20]. In fact, if a Fe_2O_3 single crystalline film is grown in low oxygen pressure, the surface is metal terminated while growth under higher oxygen pressures leads to oxygen termination. This surface would be formally unstable on the basis of electrostatic arguments [21]. However, calculations by the Scheffler group have shown that a strong rearrangement of the electron distribution as well as relaxation between the layers leads to a stabilization of the system. STM images by Weiss and co-workers corroborate the coexistence of oxygen and iron terminated layers and thus indicate that stabilization must occur. Of course, there is need for further structural characterization. For the surface of Cr_2O_3(0001) infrared spectroscopic data suggest a different termination when the clean surface is exposed to oxygen [24]. Figure 5 shows the appearance of a sharp line which develops out of a broad feature after heating the surface to room temperature. As has been discussed earlier and also supported by isotopic labeling experiments by Dillmann et al. [24] chromyl groups are formed on the surface and it was suggested that the chromium ions in the surface layer of the clean surface bind oxygen to form such chromium–oxygen double bonds. As is obvious from figure 5 there are adsorbed oxygen precursors to the chromyl formation. The width as well as frequency is indicative of an O_2^- species being adsorbed on the surface in a more or less upright position [24]. The chemistry of this species has yet to be investigated.

CO adsorption on corundum type (0001) surfaces is interesting because, opposite to checker board rocksalt type surfaces, on the (0001) surface of Cr_2O_3 CO has been shown to assume a strongly inclined almost flat adsorption geometry. Recent cluster calculations by Staemmler's group have revealed the reason for this [25]. The CO is situated between two adjacent Cr ions. This allows the carbon lone pair to interact with the positively charged Cr ions and to reduce, simultaneously, the Pauli repulsion between the CO 1π electrons and the oxygen ions by placing the molecules atop an open oxygen triangle. This leads to a more stable adsorption than by placing the molecule vertically atop a chromium ion. However, the energy differences are only of the order of a few kJ so that it is fair to assume that the molecule is rather dynamic on the surface. It is very interesting to note that CO adsorption on V_2O_3(0001) seems to show very much related behavior although the study of orientation of the molecule is not complete yet.

Another interesting case is CO_2 adsorption on Cr_2O_3 (0001) [26]. It can be almost completely suppressed when the Cr_2O_3(0001) surface is oxygen terminated with chromyl groups. On the metal-terminated surface, on the other hand, CO_2 is relatively strongly chemisorbed. The CO_2 forms a carboxyl species bound through the carbon atom to a chromium ion. Interestingly, carbonates are only easily formed when promoters such as alkali metals are present.

Water adsorption on oxide surfaces, in general, is interesting, because, under realistic conditions, water is ubiquitous. It is our experience that water adsorption is molecular on regular sites of non-polar or depolarized polar surfaces [27], although dissociative adsorption does occur [28]. Polar surfaces tend to be covered with a layer of hydroxyl groups to reduce the surface potential [4]. This has been demonstrated in the case of NiO(111) [29]. The loss of the hydroxyl layer then triggers a reconstruction of the surface. Water adsorption on MgO(100) is the best studied system so far [30–33]. The groups of Heidberg [30], Weiss and Toennies [31] have studied the system with IR, LEED and HAS. While these groups have used surfaces prepared through *in situ* cleavage, Stirniman et al. [34] have employed bulk single crystals prepared via sputtering and heating in oxygen. Their TD spectra correspond grossly to the TDS data published by Wichtendahl et al. on *in situ* cleaved MgO(100) surfaces, which are shown in figure 6 [33]. Data taken on a thin MgO film [35] reveal the essential features, although the peaks appear to be shifted significantly with respect to the temperature-calibrated data of Wichtendahl et al. The assignment of the feature at 196 K was unclear so far, although it was near at hand to assume that it is connected with the phase transition from the c(4 × 2) to the (3 × 2)pg phase which occurs at about this temperature and was reported by several groups [30,31,35]. It could be shown that the molecule density within the c(4 × 2) phase is higher than in the (3 × 2)pg phase (∼1.3 atoms and ∼1.0 atoms per magnesium surface ion, respectively) [34] so that a transition between these phases must be accompanied by a desorption peak in TDS. The TDS data of H_2O/MgO(100) in combination with data for H_2O/NiO(100) taken in our group [36] shed new light upon this question. NiO(100) and MgO(100) are isostructural with nearly identical lattice constants. According to calculations, the fields at the surfaces are very similar and, thus, desorption spectra may be expected to be similar. However, since NiO(100) and MgO(100) are similar but not identical, small differences may be expected for desorption of molecules having direct contact with the atoms of the surface. Figure 6 [36] reveals that this picture is realistic. The feature near 150 K is due to multilayer desorption and shall not be discussed here in more detail. The peak at 196 K, which corresponds to the transition from the c(4×2) phase to the (3×2)pg phase, is observed in the spectra from both surfaces, whereas the highest temperature peak, which corresponds to desorption of the (3×2)pg phase in the MgO(100) case, is found at slightly different temperatures, i.e., 225 K for NiO(100) and 239 K for MgO(100). This observation is a first hint that part of the molecules of the c(4 × 2) phase belong to the second layer and does not have contact with the oxide surface. This conclusion is supported by results of molecular dynamics simulation by the Besançon group on H_2O/MgO(100) [32]. Results are depicted in figure 7 [32]. The interesting result is that a monolayer of H_2O forms with the H_2O molecules oriented with the plane parallel to the oxide surface and with a network of H bonds within that layer, but fully disconnected from the second and higher

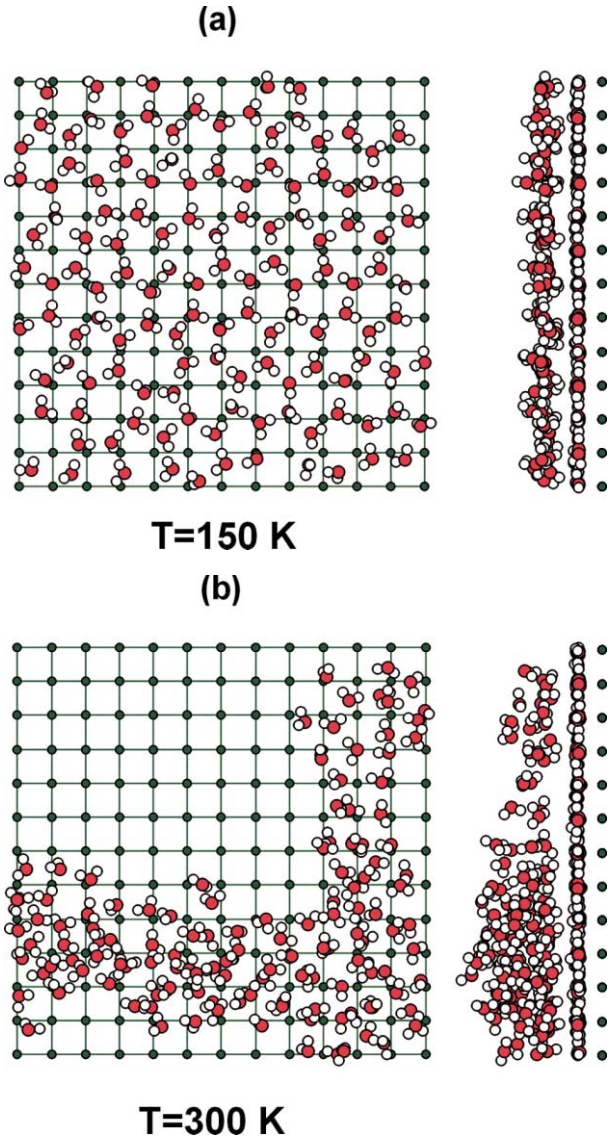

Figure 7. Simulation of water on MgO(100) at coverages higher than one monolayer at 150 K and 300 K, according to [32]. (a) Top and side views of map-shots at 150 K and (b) top and side views of map-shots at 300 K. (The first layer molecules are not represented in the top view.) The side views show that the overlayer beyond the monolayer tends to aggregate.

layers. This monolayer, which is to be identified with the (3 × 2)pg phase, completely shields the higher layers from the underlying oxide surface. Therefore, the molecules desorbing during the phase transition from the c(4 × 2) phase to the (3 × 2)pg phase may be identified as being part of the second layer, since these molecules do not feel the differences between NiO(100) and MgO(100) as documented by the data shown in figure 6.

3. Modified oxide surfaces

So far, we have considered the clean oxide surface and its reactivity. In the following we will discuss the modification of the oxide surface by deposition of metal [2,3]. The systems prepared in this way can be regarded as model sys-

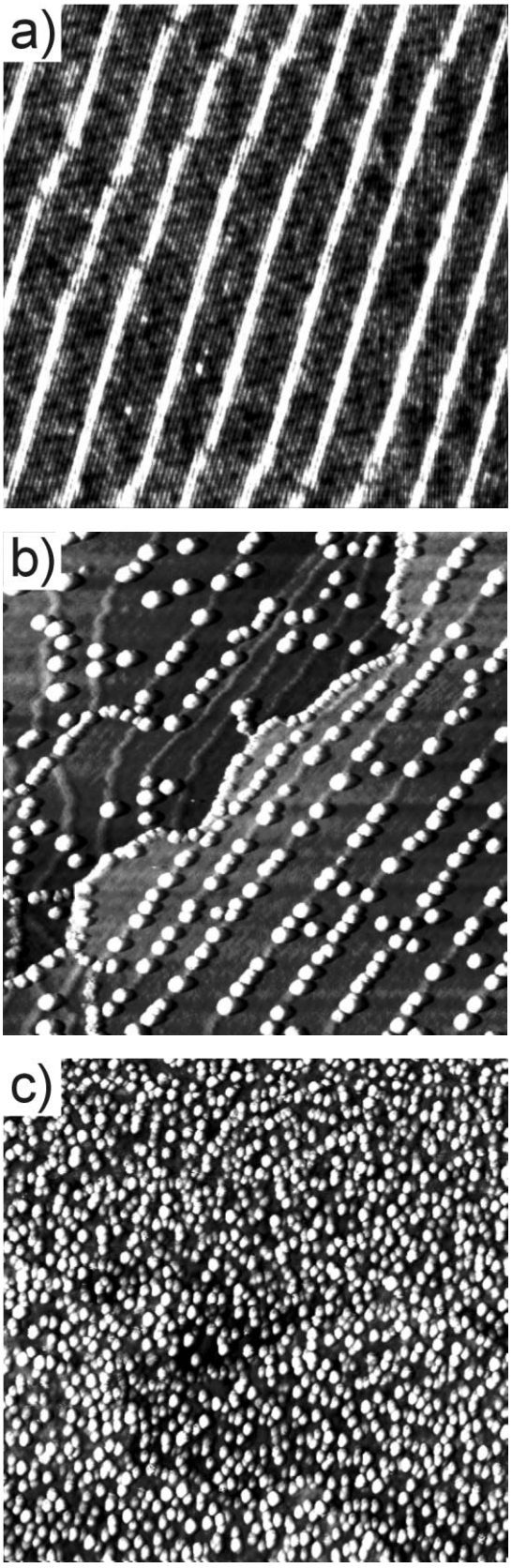

Figure 8. Scanning tunneling images (1000 × 1000 Å): (a) clean Al_2O_3/NiAl(100) film, $U = 4.2$ V, $I = 0.5$ nA; (b) after deposition of Pd (0.2 Å) at 300 K, $U = 3.1$ V, $I = 0.5$ nA; (c) after deposition of Pd (0.2 Å) at 300 K on a hydroxylated alumina film, $U = 3.1$ V, $I = 0.4$ nA.

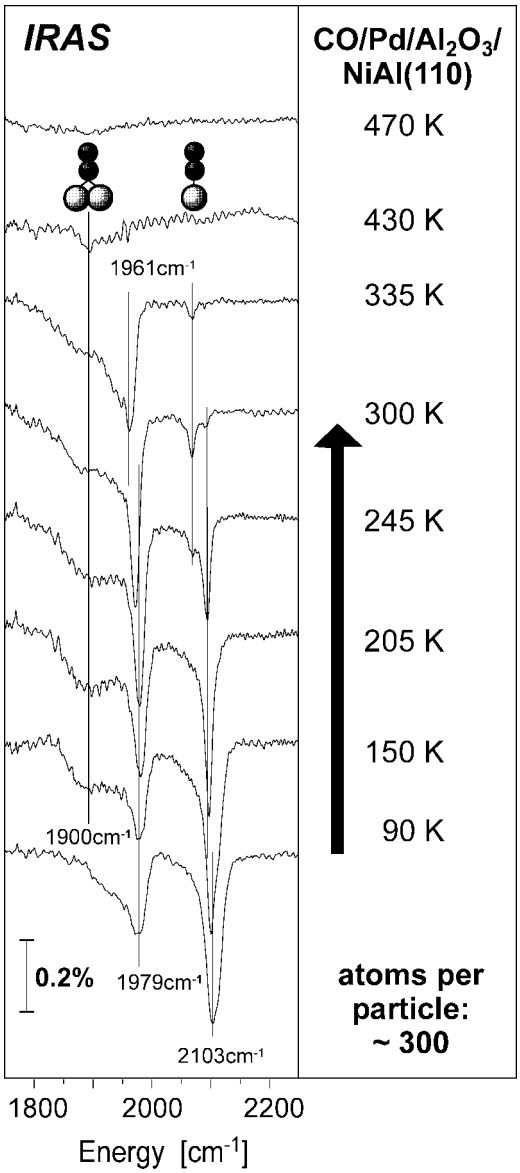

Figure 9. IRAS spectra of the CO stretching region recorded after exposing a Pd deposit on Al_2O_3/NiAl(110) with 300 atoms per aggregate on average to a saturation exposure of CO. The spectra have been recorded at various temperatures. The range of on-top and bridge bonded sites are indicated.

tems in heterogeneous catalysis [3,4]. They aim at bridging the so-called materials gap. Several groups have started to prepare such systems including Goodman [37], Henry [38], Madey [39], Møller [40] and our own group [2–4,21]. The pioneer in this field was Poppa [41] who undertook the first systematic study applying transmission electron microscopy.

Figure 8 shows STM topographs of a clean alumina film (top), after deposition of Pd at room temperature on the clean film (middle) and onto a chemically modified film which is terminated by hydroxyl groups (bottom) [3] which can be identified via vibrational spectroscopies [42].

The surface of the clean film (top) is well ordered and there are several kinds of defects present: The lines represent line defects due to anti-phase domain boundaries [43]. We know from nucleation studies that there are about 1×10^{13}

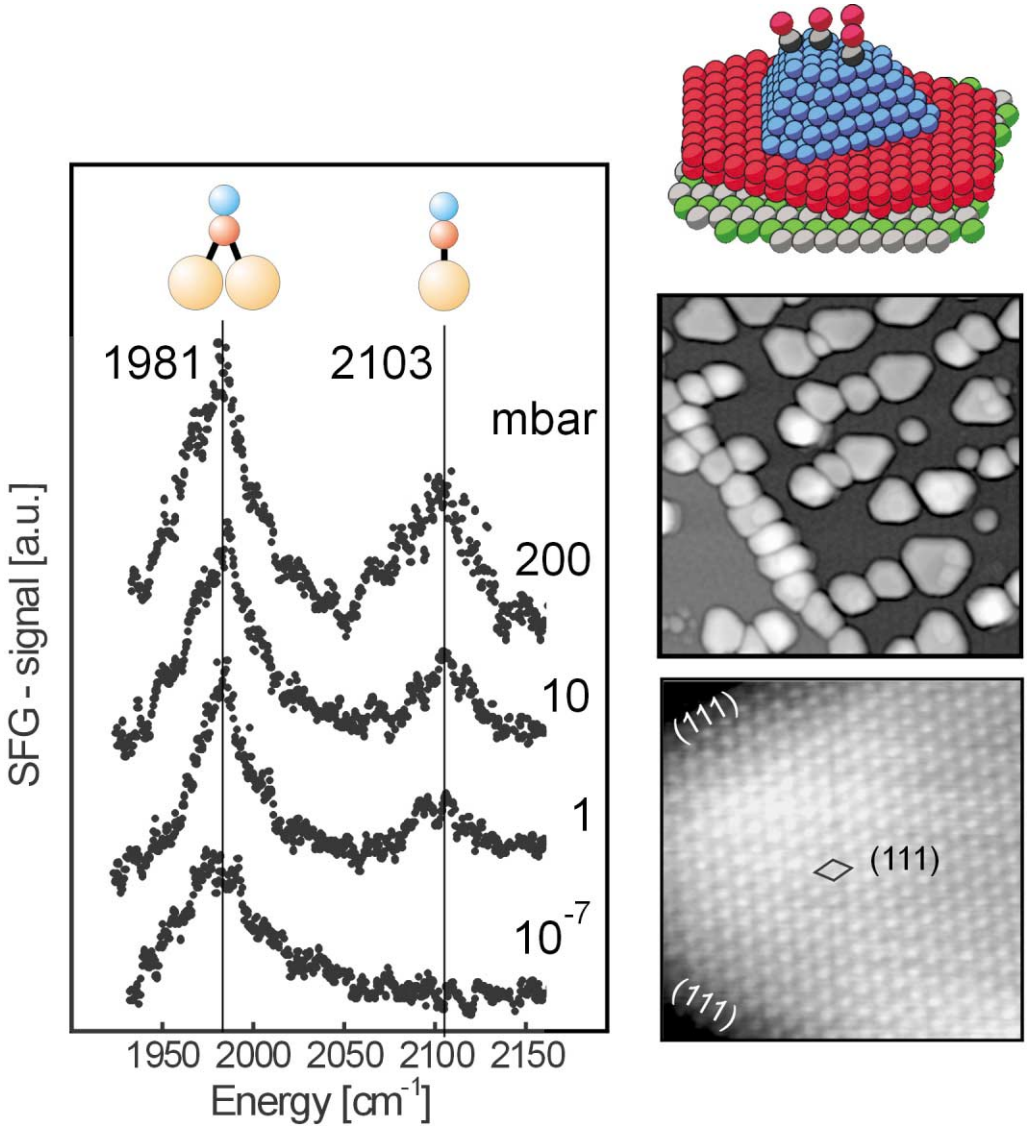

Figure 10. Vibrational spectra of the CO stretching frequency range recorded via sum-frequency generation. The spectra were recorded in UHV (bottom) and at increasing pressure towards the top. The insets show STM images of Pd deposits [45] and a schematic representation of the system.

point defects per cm^2 present as well [2]. Pd deposited at room temperature leads to aggregates residing on the domain boundaries and steps (middle). The surface of these aggregates can be imaged with atomic resolution, showing that the aggregates are crystalline and terminated by (111) and much smaller (100) facets [44,45]. The mobility of Pd under these conditions is high enough to allow nucleation at the stronger interacting line defects, whereas at 90 K the point defects determine the growth behavior. At this temperature we find aggregates statistically distributed across the entire surface of the sample.

If we deposit the same amount of Pd at room temperature onto the hydroxylated film as onto the pristine film, the dispersion of aggregates is by about an order of magnitude higher as shown in the bottom panel of figure 8 [42]. This is due to stronger interaction with the substrate which also leads to higher thermal stabilities.

We can investigate the properties of the aggregates further by studying carbon-monoxide adsorption with vibrational spectroscopy [46,47]. Figure 9 shows IR spectra of the CO stretching region of room temperature deposited aggregates at different sample temperatures. At low temperature bands characteristic for CO adsorbed in a terminal configuration as well as in multiply coordinated configurations including edges sites and terrace sites on Pd(111) as well as Pd(100) facets [48] are found. The spectra have been discussed in detail elsewhere [48]. The only important point here is that the terminally bonded CO molecules desorb at lower temperatures. The presented spectra represent saturation coverage under UHV conditions. Rupprechter et al. [8] have recently demonstrated that it is also possible to record vibrational spectra of adsorbed CO for these systems applying sum frequency generation (SFG). Figure 10 collects SFG spectra of Pd room temperature deposits saturated with CO

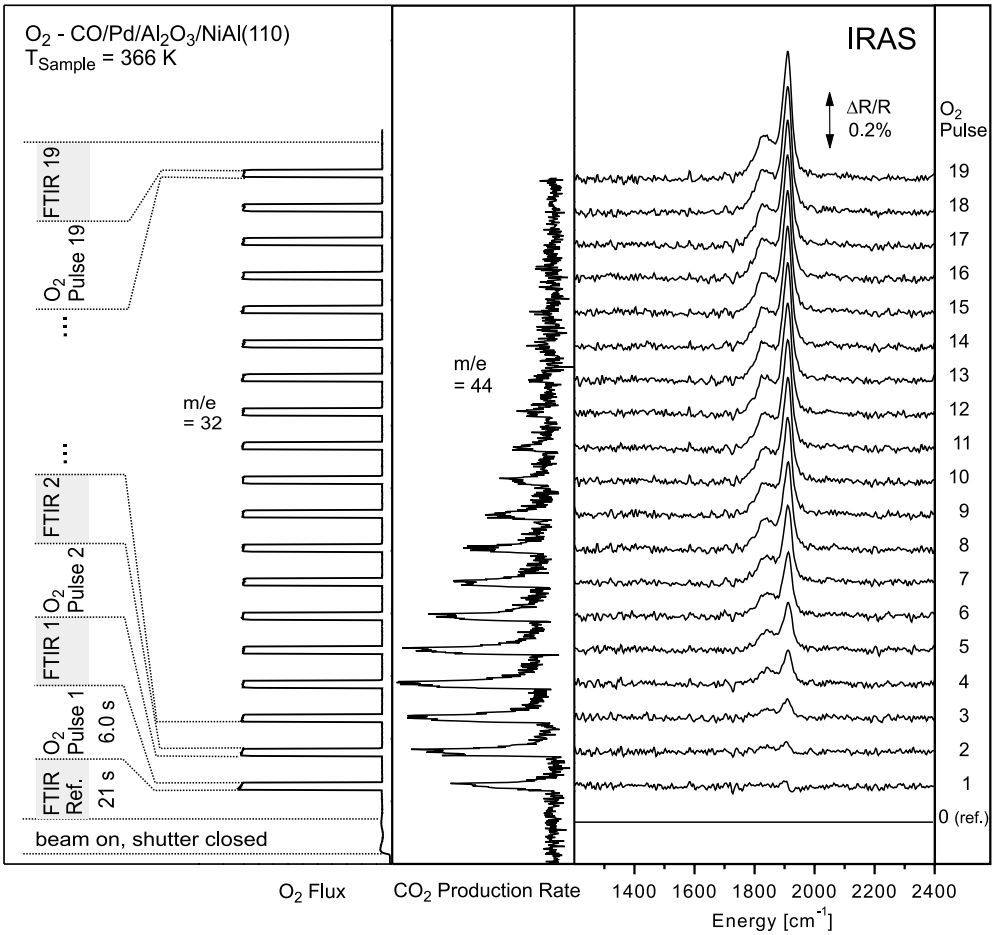

Figure 11. IRAS spectra in the CO stretching frequency regime taken while dosing an oxygen pre-covered sample of Pd/alumina deposit with CO from a chopped effective CO molecular beam. Simultaneously, the CO_2 production rate is measured with a quadrupole mass spectrometer.

at different gas pressures. Note that the resolution is limited by the present laser setup, but will be improved in the near future. Nevertheless, the bridge and the terminal configurations can be clearly differentiated. If we start under UHV conditions and choose a temperature where the terminally bonded CO molecules are unstable, and then increase the pressure slowly to 200 mbar, we see how the population of terminal CO molecules starts to increase again and reaches saturation at 0.2 bar. We note that there is no noticeable shift in the spectra taken under UHV conditions and ambient pressures. The processes are completely reversible. We feel that it cannot be stated that under pressure the system behaves fundamentally different as compared with UHV conditions [6]. On the other hand, these studies are further indications that it is possible to bridge the pressure gap also for relatively complex systems.

The next step is to investigate reactivity of aggregates and bridge the pressure gap as well with respect to reaction, by comparing UHV and higher pressures. This will also allow to ultimately investigate whether the model systems show characteristics of real catalysts systems. We have developed an experimental set up where we combine *in situ* spectroscopy with molecular beams. It is described in detail in [49]. Briefly, the surface system can be prepared under UHV conditions and then be dosed from three independent beam sources. In the experiment described below we use only one of them. The scattering of dosed molecules can be measured by two quadrupole mass spectrometers, one of which is fixed in space, the other one is rotatable allowing one to separate trapping desorption from direct channels. Thereby, also sticking probabilities can be determined. Infrared spectroscopy can be performed, simultaneously, by a fast scan FTIR-spectrometer from Bruker.

In the following we present just one example, out of several possibilities, the instrument offers. As a test reaction we have chosen CO oxidation as one of the best known surface-catalyzed reactions. A detailed study of the CO oxidation on this system will be presented elsewhere [50].

We start from a $Pd/Al_2O_3/NiAl(110)$ system, which has been stabilized by repeated O_2 and CO treatment. The surface is then saturated with CO at 366 K. Subsequently, an automated experiment is performed in which first a FTIR reference spectrum is acquired (resolution 8 cm^{-1}, acquisition time 21 s). Then O_2 is pulsed via a beam source (6 s, 6.5×10^{13} molecules $cm^{-2}\,s^{-1}$). After each pulse an IR spectrum is recorded. Simultaneously, the integral CO_2 production rate (in figure 11 corrected for the CO_2 response to the O_2 pulse from a blind experiment) and the O_2 back-

ground pressure is recorded with a quadrupole mass spectrometer fixed in space.

As a detailed analysis of the reaction kinetics is beyond the scope of this paper, we will only qualitatively point out which type of information is available from this experiment: Every CO_2 response pulse shows a rise and decay time slower than the originating O_2 pulse being rectangular on the time scale of the experiment. This is due to the limited rate of the surface reaction, the kinetics of which can be extracted from the waveform. The envelope of the waveforms represent the overall CO_2 reactive sticking coefficient of O_2 as a function of CO coverage. Due to inhibition of O_2 sticking by CO we find a rising reactive sticking coefficient at high CO coverage, before CO depletion and O_2 coadsorption leads to a decaying probability for CO_2 production. From the simultaneously acquired IR spectra information on the occupation of different sites for the consumed CO is available. Additionally, quantitative information on the surface coverage can be obtained via a coverage–absorption calibration, which can be easily performed by a simultaneous sticking coefficient/IR absorption measurement.

4. Summary

In summary, we have tried to demonstrate in which way surface science can contribute to study fundamental problems in catalysis. The emphasis is on the attempts to bridge both the materials as well as the pressure gaps.

We have investigated the structure and reactivity of clean oxide surfaces as well as metal modified oxide surfaces. In particular, the reactivity and adsorption abilities of deposited aggregates have been studied. The pressure gap has been bridged applying non-linear optical techniques and mechanistic insight has been gained with a newly designed molecular beam apparatus.

References

[1] C.B. Duke, ed., *Surface Science: The First Thirty Years* (Elsevier, Amsterdam, 1994).
[2] M. Bäumer and H.-J. Freund, Prog. Surf. Sci. 61 (1999) 127.
[3] H.-J. Freund, H. Kuhlenbeck and M. Bäumer, Adv. Catal. 45 (2000) 333.
[4] H.-J. Freund, Angew. Chem. Int. Ed. Engl. 36 (1997) 452.
[5] Ber. Bunsenges. Phys. Chem. 97 (1993).
[6] X. Su, P.S. Cremer, Y.R. Shen and G.A. Somorjai, J. Am. Chem. Soc. 119 (1997) 3994.
[7] G. Rupprechter, T. Dellwig, H. Unterhalt and H.-J. Freund, Topics Catal. 15 (2001)19.
[8] T. Dellwig, G. Rupprechter, H. Unterhalt and H.-J. Freund, Phys. Rev. Lett., in press.
[9] H. Schmalzried, *Chemical Kinetics of Solids* (VCH, Weinheim, 1995).
[10] R.K. Grasselli and J.D. Burrington, Adv. Catal. 30 (1981) 133.
[11] F. Cavani, G. Centi, F. Trifirò and R.K. Grasselli, Catal. Today 3 (1988) 185.
[12] P.A. Agaskar, L. DeCaul and R.V. Grasselli, Catal. Lett. 23 (1994) 339.
[13] B. Tepper, Ph.D. thesis, in preparation.
[14] A.-C. Dupuis, Ph.D. thesis, in preparation.
[15] K. Hermann, M. Witko, R. Druzinic, A. Chakrabarti, B. Tepper, M. Elsner, A. Gorschlüter, H. Kuhlenbeck and H.-J. Freund, J. Electron Spectrosc. Relat. Phenom. 98–99 (1999) 245.
[16] M. Figlarz, Progr. Sol. State Chem. 19 (1989) 1.
[17] G. Renaud, Surf. Sci. Rep. 32 (1998) 1.
[18] F. Rohr, M. Bäumer, H.-J. Freund, J.A. Mejias, V. Staemmler, S. Müller, L. Hammer and K. Heinz, Surf. Sci. 372 (1997) L291;
F. Rohr, M. Bäumer, H.-J. Freund, J.A. Mejias, V. Staemmler, S. Müller, L. Hammer and K. Heinz, Surf. Sci. 389 (1997) 391.
[19] S.K. Shaikhoutdinov and W. Weiss, Surf. Sci. 432 (1999) L627.
[20] X.-G. Wang, W. Weiss, S.K. Shaikhoutdinov, M. Ritter, M. Petersen, F. Wagner, R. Schlögl and M. Scheffler, Phys. Rev. Lett. 81 (1998) 1038.
[21] H.-J. Freund, Faraday Discuss. 114 (1999) 1.
[22] N.M. Harrison, X.-G. Wang, M. Muscat and M. Scheffler, Faraday Discussions 114 (1999) 305.
[23] K. Wolter, D. Scarano, J. Fritsch, H. Kuhlenbeck, A. Zecchina and H.-J. Freund, Chem. Phys. Lett. 105 (2000) 295.
[24] B. Dillmann, F. Rohr, O. Seiferth, G. Klivenyi, M. Bender, K. Homann, I.N. Yakovkin, D. Ehrlich, M. Bäumer, H. Kuhlenbeck and H.-J. Freund, Faraday Discuss. 105 (1996) 295.
[25] M. Pykavy, V. Staemmler, O. Seiferth and H.-J. Freund, Surf. Sci., submitted.
[26] O. Seiferth, K. Wolter, B. Dillmann, G. Klivenyi, H.-J. Freund, D. Scarano and A. Zecchina, Surf. Sci. 421 (1999) 176.
[27] D. Cappus, C. Xu, D. Ehrlich, B. Dillmann, C.A. Ventrice, Jr., K. Al-Shamery, H. Kuhlenbeck and H.-J. Freund, Chem. Phys. 177 (1993) 533.
[28] M.A. Henderson and S.A. Chambers, Surf. Sci. 449 (2000) 135.
[29] F. Rohr, K. Wirth, J. Libuda, D. Cappus, M. Bäumer and H.-J. Freund, Surf. Sci. 315 (1994) L977.
[30] J. Heidberg, B. Redlich and D. Wetter, Ber. Bunsenges. Phys. Chem. 99 (1995) 1333.
[31] D. Ferry, A. Glebov, V. Senz, J. Suzanne, J.P. Toennies and H. Weiss, J. Chem. Phys. 105 (1996) 1697.
[32] A. Marmier, P.N.M. Hoang, S. Picaud, C. Girardet and R.M. Lynden-Bell, J. Chem. Phys. 109 (1988) 3245.
[33] R. Wichtendahl, M. Rodriguez-Rodrigo, U. Härtel, H. Kuhlenbeck and H.-J. Freund, Phys. Stat. Sol. 173 (1999) 93.
[34] M.J. Stirniman, C. Huang. R.C. Smith, J.A. Joyce and B.D. Kay, J. Chem. Phys. 105 (1996) 1295.
[35] C. Xu and D.W. Goodman, Chem. Phys. Lett. L65 (1997) 341.
[36] R. Wichtendahl, Ph.D. thesis, Freie Universität Berlin (1999).
[37] D.W. Goodman, Surf. Rev. Lett. 2 (1995) 9.
[38] C.R. Henry, Surf. Sci. Rep. 31 (1998) 231.
[39] U. Diebold, J.-M. Pan and T.E. Madey, Surf. Sci. 331 (1995) 845.
[40] M.C. Wu and P.J. Møller, Surf. Sci. 221 (1989) 250.
[41] H. Poppa, Catal. Rev. Sci. Eng. 35 (1993) 359.
[42] M. Heemeier, M. Frank, J. Libuda, K. Wolter, H. Kuhlenbeck, M. Bäumer and H.-J. Freund, Catal. Lett. 68 (2000) 19.
[43] J. Libuda, F. Winkelmann, M. Bäumer, H.-J. Freund, T. Bertrams, H. Neddermeyer and K. Müller, Surf. Sci. 318 (1994) 61.
[44] N. Ernst, B. Duncombe, G. Bozdech, M. Naschitzki and H.-J. Freund, Ultramicroscopy 79 (1999) 231.
[45] K. Højrup Hansen, T. Worren, S. Stempel, E. Laegsgaard, M. Bäumer, H.-J. Freund, F. Besenbacher and I. Stensgaard, Phys. Rev. Lett. 83 (1999) 4120.
[46] M. Frank, R. Kühnemuth, M. Bäumer and H.-J. Freund, Surf. Sci. 427 (1999) 288.
[47] M. Frank and M. Bäumer, Phys. Chem. Chem. Phys., to be published.
[48] K. Wolter, O. Seiferth, H. Kuhlenbeck, M. Bäumer and H.-J. Freund, Surf. Sci. 399 (1998) 190.
[49] J. Libuda, I. Meusel, J. Hartmann and H.-J. Freund, Rev. Sci. Instr., submitted.
[50] I. Meusel, J. Libuda, J. Hartmann and H.-J. Freund, to be published.